RESEARCH ARTICLE

WILEY

Identification of cuproptosis-related subtypes and characterization of the tumor microenvironment landscape in head and neck squamous cell carcinoma

Juntao Huang[1,2] 🔟 | Ziqian Xu[3] | Zhechen Yuan[1,2] | Lixin Cheng[1,2] | Chongchang Zhou[1,2] 🔟 | Yi Shen[1,2]

[1]Department of Otolaryngology Head and Neck Surgery, Ningbo Medical Center Lihuili Hospital, The Affiliated Lihuili Hospital of Ningbo University, Ningbo, China

[2]School of Medicine, Ningbo University, Ningbo, China

[3]Department of Dermatology, Shanghai General Hospital, Shanghai Jiao Tong University School of Medicine, Shanghai, China

Correspondence
Yi Shen, Department of Otolaryngology Head and Neck Surgery, Ningbo Medical Center Lihuili Hospital, The Affiliated Lihuili Hospital of Ningbo University, Ningbo, Zhejiang, China.
Email: tyzdhs@163.com

Abstract

Background: Cuproptosis is considered a novel copper-dependent cell death model. In this study, we established a novel scoring system based on 10 cuproptosis-related genes (CRGs) to predict the prognosis and immune landscape of head and neck squamous cell carcinoma (HNSCC).

Methods: The RNA-seq data of HNSCC patients were downloaded from the GEO and TCGA databases and were merged into a novel HNSCC cohort. Multiomics landscape analyses were conducted, including tumor mutation burden (TMB), copy number variations and the interaction network of CRGs. Patients were then divided into different cuproptosis subtypes based on the expression of 10 CRGs and subsequently regrouped into novel gene clusters referring to differentially expressed genes. A cuproptosis score (CS) system was established using principal component analysis. The CIBERSORT, ssGSEA and ESTIMATE algorithms were used to assess the tumor immune microenvironment. Moreover, the immunotherapeutic and chemotherapeutic responses were assessed.

Results: Patients were divided into three cuproptosis subtypes and subsequently regrouped into three gene clusters, reflecting different immune infiltration. Assessed by the CS system, those with higher CSs exhibited worse prognosis and higher TMB frequency. Nevertheless, the immune-related analysis revealed patients in the low-CS group appeared immunosuppressive and easily suffered from immune escape. High CSs possibly show high expression of immune checkpoint genes and enhance chemotherapy sensitivity to cisplatin, docetaxel, and gemcitabine.

Conclusion: We established a novel scoring system to predict the prognosis and immune landscape of HNSCC patients. This signature exhibits satisfactory predictive effects and the potential to guide comprehensive treatment for patients.

1 | INTRODUCTION

Head and neck squamous cell carcinoma (HNSCC) is considered the most common type of head and neck cancer, with increasing diagnosed cases per year and poor prognosis.[1,2] To eliminate the tumor tissue and prolong the survival time for patients, conventional treatment, including surgery, radiotherapy, and chemotherapy, was applied; nevertheless, the prognosis remained unsatisfactory.[3,4] Especially for advanced HNSCC, the survival rate is approximately as low as 50%.[5,6] Hence, it is crucial to explore novel methods to predict prognosis and guide treatment for patients.

Immune checkpoint inhibitor (ICI) antibodies are a novel treatment for HNSCC patients and have substantially improved prognosis by identifying and eliminating tumor cells and activating patients' immune defense systems.[7–9] However, patients exhibit different immunotherapeutic responses due to differences in the tumor microenvironment (TME), and a minority of patients receive benefits.[10] According to compelling evidence, the programmed cell death process is associated with the immunotherapy response and plays a core role in tumor progression.[2,11]

Copper plays an important role in organisms. The concentrations influence the biological process and induce cell death.[12] As reported by Tsvetkov et al, cuproptosis is a novel copper-dependent cell death process that is distinct from known death mechanisms and dependent on mitochondrial respiration regulated by targeting lipoylated components of the tricarboxylic acid (TCA) cycle.[12] It can be induced by mitochondrial stress, lipoylated mitochondrial enzyme aggregation and Fe-S cluster protein loss.[13,14] As a novel cell death model, cuproptosis shows great potential and prospects in the treatment of tumors. However, there is a lack of studies investigating the relationship between cuproptosis and HNSCC. In this study, we divided HNSCC patients into novel molecular subtypes based on the expression of 10 cuproptosis-related genes (CRGs) and subsequently constructed a novel scoring system to predict the prognosis and immune landscape of HNSCC according to the differentially expressed genes (DEGs) among the molecular subtypes.

2 | METHODS AND MATERIALS

2.1 | Obtaining HNSCC datasets and clinical data

Head and neck squamous cell carcinoma gene expression datasets with detailed clinical information were downloaded from the Gene Expression Omnibus (GEO) and The Cancer Genome Atlas (TCGA) databases (last assessed: 1 May 2022). A total of three available datasets, including GSE41613 and GSE65858 from the GEO database and the RNA sequencing (RNA-seq) transcriptome data of the TCGA-HNSC dataset from the TCGA database, were used for further analysis. For the TCGA-HNSC cohort, the gene expression matrix was obtained as transcripts per million (TPM). Background adjustment and quantitative normalization were performed, and the batch effect was removed to construct a novel merge gene expression matrix. To decrease the potential bias, we excluded patients with short overall survival (OS) values, which were less than 30 days, or missing OS values.

2.2 | Multiomics landscape analysis based on CRGs in the TCGA-HNSC dataset

Referring to Tsvetkov et al's study, we selected 10 core CRGs from the lipoic acid (LA) pathway (including FDX1, LIPT1, LIAS and DLD) and the pyruvate dehydrogenase (PDH) complex (consisting of DLAT, PDHA1, PDHB, MTF1, GLS and CDKN2A) for further analysis.[12] The expression of these 10 genes between 504 HNSCC samples and 44 normal samples was compared by the utilization of the "limma" R package. The somatic mutation data of these 10 CRGs and tumor mutation burden (TMB) were analyzed and evaluated, which are reflected in the waterfall plot. In addition, the copy number variation (CNV) frequency of CRGs was assessed. Moreover, a univariate Cox (uni-Cox) analysis was subsequently conducted to identify prognostic CRGs related to survival, and an interaction network was established to reveal the correlation among these 10 CRGs.

2.3 | Molecular subtypes based on the expression of CRGs

Based on the expression of CRGs, patients were subsequently divided into different subtypes with the use of the "ConsesusClusterPlus" R package. Kaplan–Meier survival analysis was also conducted to compare the OS values in clusters. Moreover, a heatmap plot was utilized to reflect the relationship between CRG expression and clinical characteristics.

2.4 | Functional enrichment analysis

Gene set variation analysis (GSVA) was performed to compare the differentially enriched pathways (adjusted p value < 0.05) of the cuproptosis subtypes in accordance with the assisted gene set (c2.cp.kegg.v6.2.-symbols) obtained from the Molecular Signature

Database.[15] The differentially expressed genes (DEGs) of the cuproptosis subtypes were then compared in each of the two clusters and identified with the criteria of adjusted *p* value < 0.05. Based on the intersection of these DEGs, gene ontology (GO) analysis was conducted to explore enriched GO terms, including biological processes (BPs), cellular components (CCs) and molecular functions (MFs). In addition, Kyoto Encyclopedia of Gene and Genomes (KEGG) pathway analysis was used to identify the potential pathways enriched in DEGs. All enriched GO and KEGG terms were considered significant, while the p-value and *q*-value were < 0.05.

2.5 | Assessment of the immune landscape of cuproptosis clusters

The immune cell subsets of each HSNCC sample were calculated using the CIBERSORT method. Moreover, the immune infiltration statuses and immune functions were analyzed with the use of a single sample gene set enrichment analysis (ssGSEA) algorithm. In addition, to assess and compare the tumor immune microenvironment in different cuproptosis clusters, we utilized the "estimate" R package to calculate the immune score, stromal score, ESTIMATE score and tumor purity of each HNSCC sample.

2.6 | Establishment of cuproptosis-related DEG clusters and cuproptosis scores

The DEGs of interest in cuproptosis clusters were then identified and selected with uni-Cox regression analysis. Based on the expression of these prognostic DEGs, the HNSCC cohort was divided into novel gene clusters. Kaplan–Meier (K-M) survival analysis and immune infiltration were also conducted as in the cuproptosis clusters, and a heatmap plot was used to show the correlation of cuproptosis clusters, gene clusters, CRG expression, and clinical features. In addition, principal component analysis (PCA) was conducted to establish a novel cuproptosis signature score system. For each sample of the HNSCC dataset, the cuproptosis score was calculated using the following formula: cuproptosis score (CS) = $\sum PC1^i + PC2^i$.[16,17] Furthermore, based on the cut-point survival analysis, patients were regrouped into low-CS and high-CS groups.

2.7 | Correlation of CSs and subtypes

The correlations of the cuproptosis clusters, gene clusters, CS groups and survival status are shown in the Sankey diagram. Subsequently, the differences in the survival status of the CSs were analyzed and compared. In addition, survival analysis was conducted between the two CS groups and compared in accordance with different clinical characteristics, including age (<60 or ≥60), gender (male or female) and clinical stage (stages I–II or stages III–IV).

2.8 | Correlation of CSs and TMB

The 20 topmost mutated genes in both the low-CS and high-CS groups are shown in the waterfall plots. The total mutation counts of each HNSCC sample were analyzed, and the tumor mutation burden (TMB) frequency was compared between the two CS groups. Spearman's correlation analysis was applied to explore the relationship between CS and TMB. Survival analysis was also conducted to investigate and compare the OS values for patients with different CSs and TMB frequencies.

2.9 | Assessment of immunotherapy and chemotherapy

Subsequently, the efficacy of clinical immunotherapy and chemotherapy was further explored. The correlation between CSs, immune cells and immune functions was assessed by the Pearson correlation test based on the ssGESA method. In addition, the expression of ICI-related genes, including PD-1, PD-L1 and CTLA, was compared between the low-CS and high-CS groups. Tumor immune dysfunction and exclusion (TIDE)-related scores, including TIDE scores, T-cell dysfunction scores and T-cell exclusion scores, were predicted by the TIDE database and compared to evaluate the effectiveness of the immunotherapy response.

Four conventional chemotherapeutic agents, including cisplatin, paclitaxel, docetaxel and gemcitabine, were selected to predict the drug sensitivity and effectiveness of chemotherapy based on the value of half-maximum inhibitory concentration (IC50) via the "pRRophetic" R package.

3 | RESULTS

3.1 | Multiomics landscape analysis in the TCGA-HNSC cohort

With the utilization of the "limma" R package, the differentially expressed CRGs are shown in Figure 1A, including DLAT, PDHB, GLS and CDKN2A. Among them, GLS and CDKN2A were considered upregulated in tumor samples; nevertheless, DLAT and PDHB were downregulated. Accordingly, the overall mutation rate of 10 CRGs was 22.75%, and CDKN2A appeared to have the highest mutation rate (20% total). (Figure 1B) In addition, CNV analysis revealed that FDX1, DLAT and CDKN2A perform copy number deletions (Figure 1C), and the locations of these 10 CRGs on the chromosomal rcircos are shown in Figure 1D. Moreover, the interaction and interconnection of 10 CRGs and their efficacy on the patient OS are described in Figure 1E.
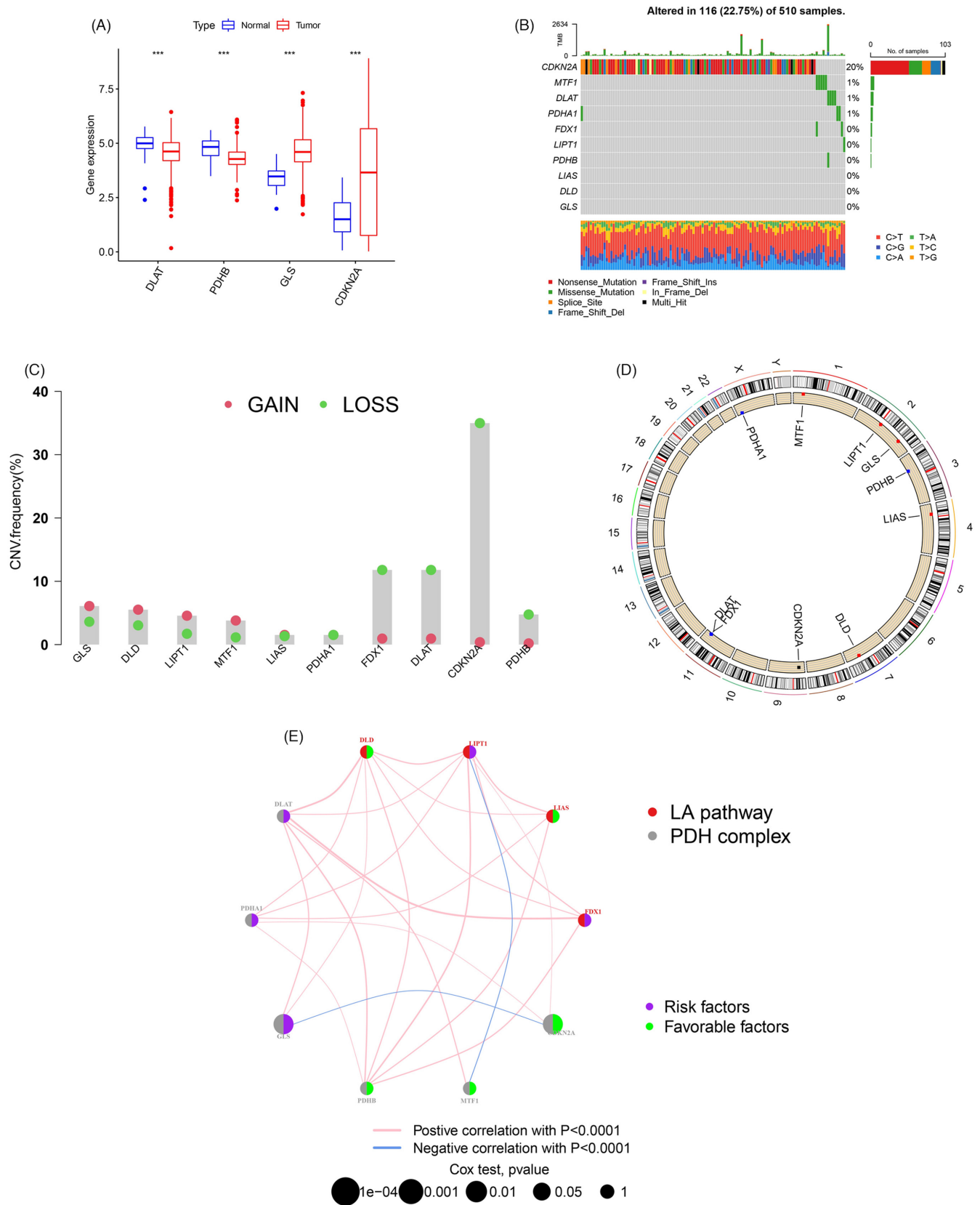
FIGURE 1 Multiomics analysis of CRGs in TCGA-HNSC. (A) Boxplots of differential expressed CRGs; (B) Tumor mutation frequency of CRGs; (C) CNV frequency of CRGs in TCGA-HNSC cohort; (D) The location of PRGs with CNV mutation on chromosomes; (E) Interaction among CRGs in HNSCC patients.

3.2 | Subtypes based on the expression of CRGs

Based on the expression of 10 CRGs, patients were subsequently divided into three clusters with the use of the "ConsensusCluster" R package. The K-M survival indicated that these three clusters had significantly different OS ($p = 0.047$), which suggested that patients in cluster A had the worst prognosis. (Figure 2A) The heatmap plot reflected different expressions of CRGs, and the CDKN2A gene was mostly upregulated in cluster B but downregulated in cluster A. (Figure 2B) In addition, the GSVA analysis determined that there were many more differentially enriched KEGG pathways between cluster B and cluster C. (Figure 2C and Figures S1 and S2) Moreover, according to the results of CIBERSORT, cluster B had more immune cell infiltration, including CD8+ T cells, activated CD4+ T cells and M1 macrophages. (Figure 2D) The results of ssGSEA also supported the CIBERSORT analysis and determined that cluster B was more associated with APC coinhibition; nevertheless, cluster C was more associated with the activation of immune functions (e.g., CCR). (Figure 2E,F) In addition, referring to the application of the "estimate" R package, differences in the TME scores among the three cuproptosis clusters were investigated and are summarized in Figure 2G. As shown in the boxplots, patients in cluster C had the highest immune scores and the lowest tumor purity, and cluster B had the lowest stromal scores, but there were no significant differences among the three cuproptosis clusters for the ESTIMATE score.

3.3 | Gene clusters based on prognostic DEGs

According to the Venn diagram, there were 112 DEGs among the three clusters. (Figure S3) GO and KEGG enrichment analyses suggested that these 112 DEGs may be mostly enriched in the DNA replication of BPs, chromosomal region of CCs, catalytic activity acting on DNA of MFs and DNA replication pathways. (Figures S4 and S5) Among them, eight genes were considered associated with patient survival, including CDKN2A, PRELID2, ANP32B, MRPL47, CCDC59, WDR90, NLRX1 and KCNK6. (Figure 3A) Based on the expression of these eight DEGs, the HNSCC patients were then regrouped into three gene clusters, and the K-M curves suggested significant differences in OS among these gene clusters. (Figure 3B) A heatmap of the gene clusters showed the relationship among gene expression, cuproptosis clusters, gene clusters and clinical characteristics. (Figure 3C) In addition, the boxplot in Figure 3D reflected the CRG distribution in three gene clusters, indicating that cluster A had the highest expression of GLS and cluster C had the highest expression of FDX1, DLAT and MTF1. However, cluster B displayed the most high CRG expression, including LIAS, LIPT1, PDHA1 PDHB and CDKN2A. Furthermore, as reflected by the results of CIBERSORT and ssGSEA, cluster B and cluster C represented much more enriched immune infiltration and immune functions. (Figure 3E–G) By comparing TME scores among the three gene clusters, patients in gene cluster B were assessed to have the lowest immune scores, stromal scores, ESTIMATE scores and the highest tumor purity;

nevertheless, there was no difference in TME scores between clusters A and C. (Figure 3H).

3.4 | Correlation of CSs and subtypes

Concerning the PCA, patients in the HNSCC cohort were assessed with the cuproptosis score and were divided into low-CS and high-CS groups. As shown in the Sankey plot, the correlations of cuproptosis clusters, gene clusters, CS groups and survival status were revealed. (Figure 4A) The K-M survival analysis, as well as barplots and boxplots, suggested that patients with high CSs had a worse prognosis. (Figure 4B,C) Comparing the OS between the low-CS and high-CS groups with different clinical characteristics, patients in the low-CS group exhibited better prognosis with clinical features of age ≥60, males, females or stages III–IV. However, there were no differences between the two CS groups in groups of age <60 and stages I–II. (Figure 4D–I).

3.5 | Correlation between CSs and TMB

Waterfall plots of the TMB in the low-CS and high-CS groups are shown in Figure 5A,B. Based on the Wilcoxon signed-rank test and Spearman's correlation analysis, patients in the low-CS group had a lower TMB than those in the high-CS group, and CSs were positively correlated with TMB. (Figure 5C,D) Moreover, considering the survival analysis of TMB, patients with high TMB had a worse prognosis, especially when combined with high CSs. (Figure 5E,F).

3.6 | TME, immunotherapeutic and chemotherapeutic response

As suggested by the CIBERSORT algorithm, the CSs exhibited a positive correlation with naive B cells, monocytes and activated CD4+ memory T cells infiltration. In contrast, gamma delta T cells, activated dendritic cells, resting dendritic cells, neutrophils and plasma cells were negatively associated with CSs. (Figure 6A,B) The correlation analysis based on ssGSEA also supported the CIBERSORT results regarding immune cell infiltration, which showed that CSs had a positive correlation with activated B cells, CD4+ T cells and CD8+ T cells. (Figure 6C) In addition, CSs were positively correlated with most immune functions. (Figure 6D) However, there were no significant differences in TME scores between the low-CS and high-CS groups. (Figure 6E) Regarding the expression of ICI genes, patients in the high-CS group exhibited higher expression of PD-1 and CTLA4 than those in the low-CS group. (Figure 7A) Moreover, referring to the analysis of TIDE-related scores, patients with high CSs had significantly higher exclusion scores, lower TIDE scores and lower T cell dysfunction scores than low-CS patients. (Figure 7B) Given these findings, patients with high CSs may possibly be more sensitive to immunotherapy.
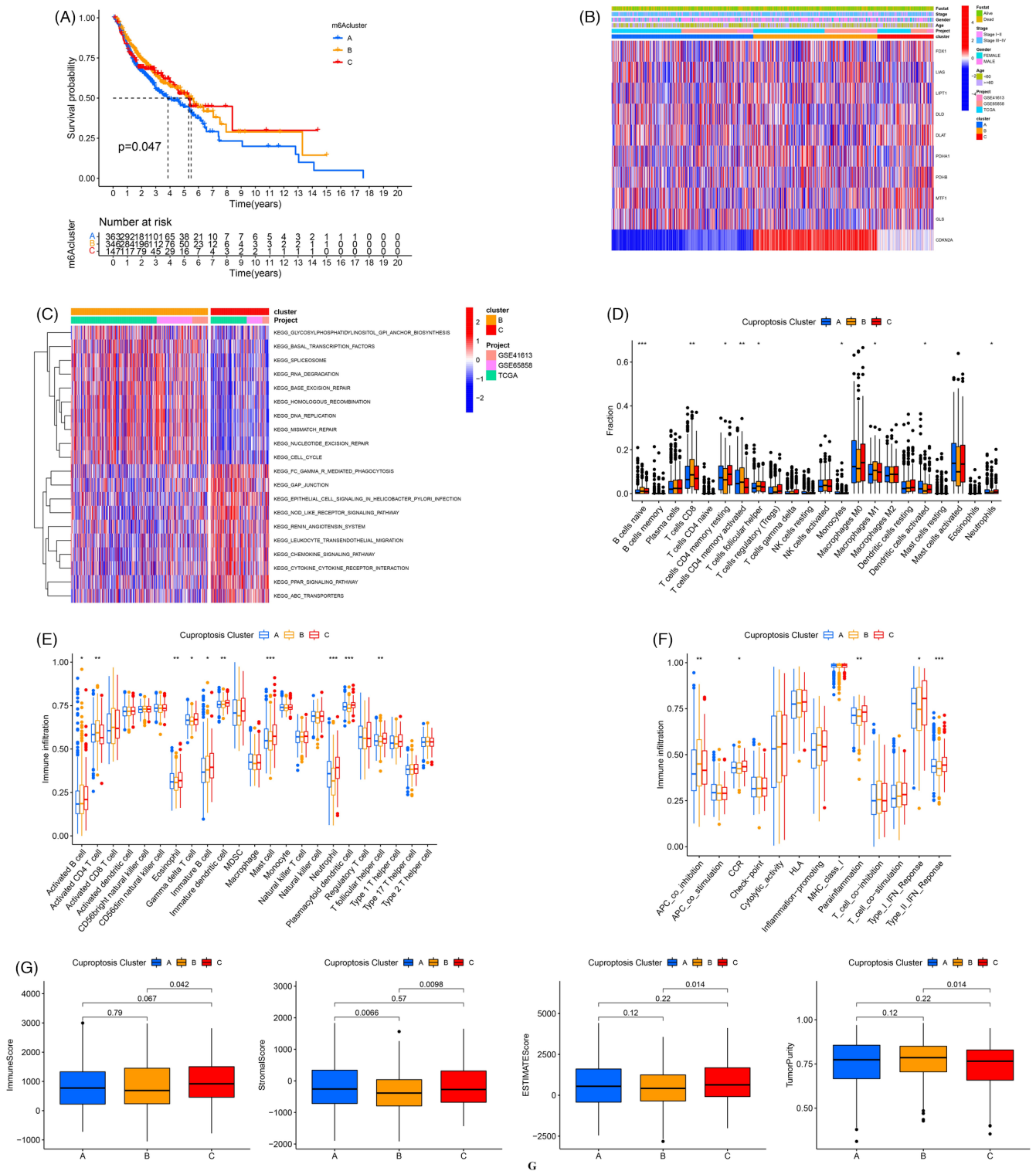
FIGURE 2 Subtypes based on the expression of CRGs. (A) Kaplan-Meier survival analysis among three clusters; (B) Heatmap of CRGs, clinical features in subtypes; (C) GSVA analysis between cluster B and C; (D) CIBERSORT analysis; (E) Immune cell infiltration based on ssGSEA; (F) Immune function analysis in cuproptosis clusters; (G) TME scores based on ESTIMATE algorithm.

Similarly, we also assessed the drug sensitivity of four conventional chemotherapeutic agents. Based on the IC50 values, the CSs were negatively correlated with the IC50 values of cisplatin, docetaxel, and gemcitabine, which indicated that patients with high CSs were more sensitive to these three drugs. However, patients in the low-CS group exhibited lower IC50 values and higher sensitivity to paclitaxel. (Figure 7C,D).
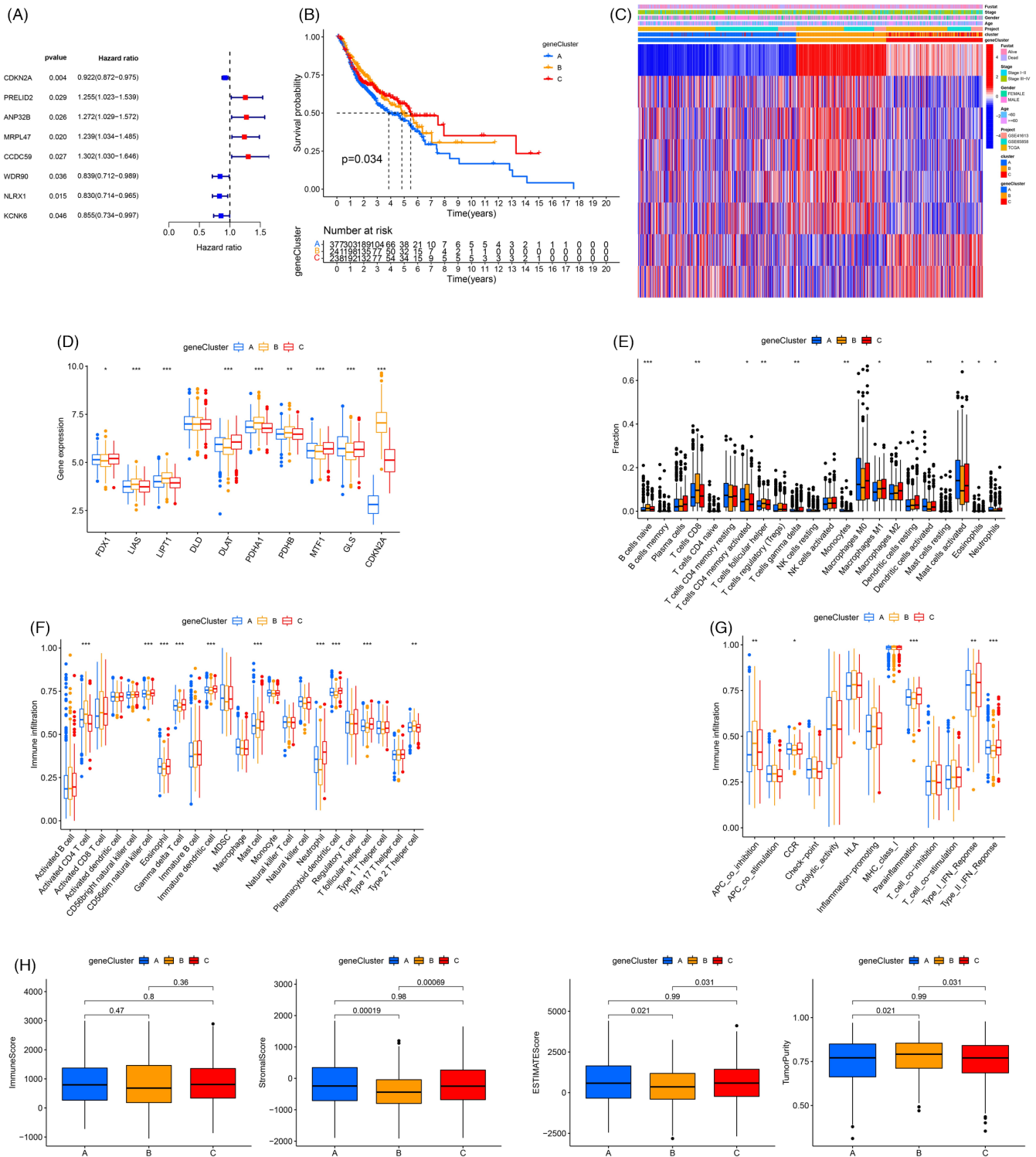
FIGURE 3 Gene cluster based on prognostic DEGs. (A) Forest plot of prognostic DEGs. (B) Kaplan-Meier survival analysis among three gene clusters; (C) Heatmap of CRGs, clinical features, cuproptosis subtypes and gene clusters; (D) Expression of CRGs in gene clusters; (E) CIBERSORT analysis in gene clusters; (F) Immune cell infiltration in gene clusters; (G) Immune function in gene clusters; (H) TME scores in gene clusters.

4 | DISCUSSION

Considering the poor prognosis and therapeutic efficacy for advanced HNSCC patients, a novel accurate prognostic model is crucial

to predict prognosis and guide individualized and precise treatment.[1,2] Previous studies have determined that the programmed cell death process is involved in metabolizing tumor cell biological processes of proliferation, migration and invasion and the TME, which can be
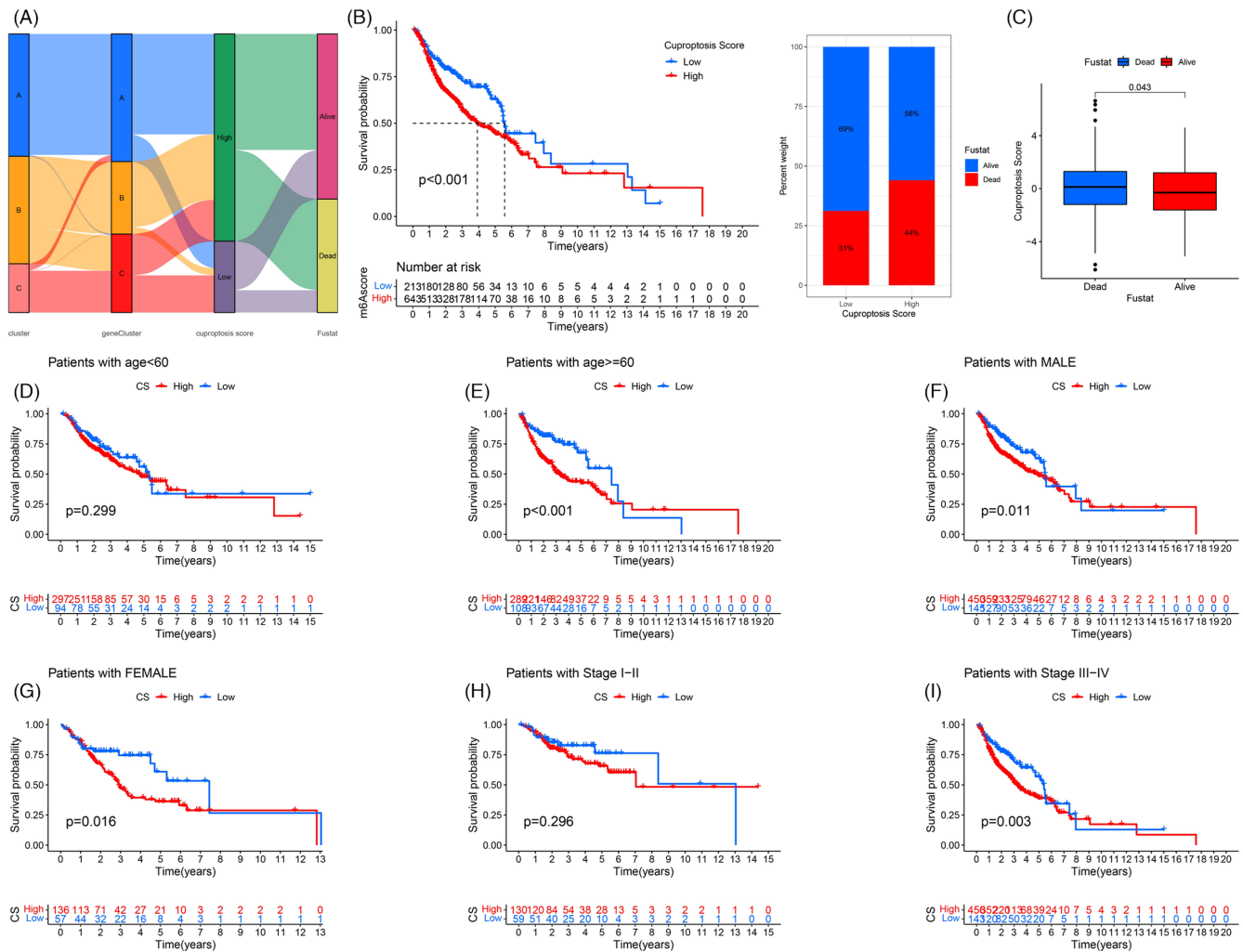
FIGURE 4 Correlation of CSs and subtypes. (A) Sankey plot revealing the relationship; (B) K-M analysis between the low-CS and high-CS groups. (C) The survival distinction of patients in the CS groups. (D–I), Relationship between CSs and clinical subtypes of HNSCC patients.

considered novel prognostic biomarkers and potential therapeutic targets.[18–20] Referring to a recent study investigated by Tsvetkov et al.[12] cuproptosis was determined to be a novel copper-induced cell death model and considered a potential therapeutic prospect for tumor patients. In this study, we explored the correlation between cuproptosis and HNSCC and constructed a novel scoring system to predict the prognosis and therapeutic effects for patients.

Compared to conventional prognostic signatures, in this study, we focused on DEGs among cuproptosis clusters to establish the CS system instead of the differential expression of CRGs in HNSCC patients. The multiomics analysis revealed a comprehensive landscape of the somatic mutation, CNV frequency, chromosome location and interaction associated with CRGs in the TCGA-HNSC cohort. After dividing patients into three subtypes based on the expression of CRGs, the three cuproptosis clusters exhibited different survival and outcomes and biological function activity in HNSCC. As indicated by the GSVA analysis, most of the different pathways among the three cuproptosis subtypes were associated with DNA replication and metabolism, which are considered to play important roles in tumors. Based on the ESTIMATE, CIBERSORT and ssGSEA algorithms, diverse TME characterizations identified that cuproptosis cluster A possibly exhibited the

worst immunotherapeutic response with lower immune scores, less immune cell infiltration and enriched immune functions.[21,22]

To further assess the effects of 10 CRGs, three gene clusters were identified as cuproptosis patterns for HNSCC patients based on eight DEGs. The survival analysis revealed different OS, and immune-related analysis reflected a distinct tumor immune microenvironment. Among the eight DEGs, CDKN2A was considered the prognostic CRG that was upregulated in HNSCC samples. Previous studies determined that the CDKN2A gene is a common mutation of the tumor suppressor and checkpoint mediator in HPV-negative HNSCC.[23] Similarly, CDKN2A inactivation also appears with frequent copy number alterations in smoking-related HNSCCs. Therefore, CDKN2A plays important roles in the prognosis of HSNCC patients.[24]

Based on the PCA, each HNSCC patient was assessed with CSs and regrouped into low-CS and high-CS groups. As indicated, K-M survival analysis revealed that high CSs increased the risks and led to worse prognosis for HNSCC patients. The clinical subgroup comparisons of age, sex and clinical stage suggest that the prognostic patterns were effective in all subgroups except the age <60 and stage I-II subgroups, which may be caused by low case
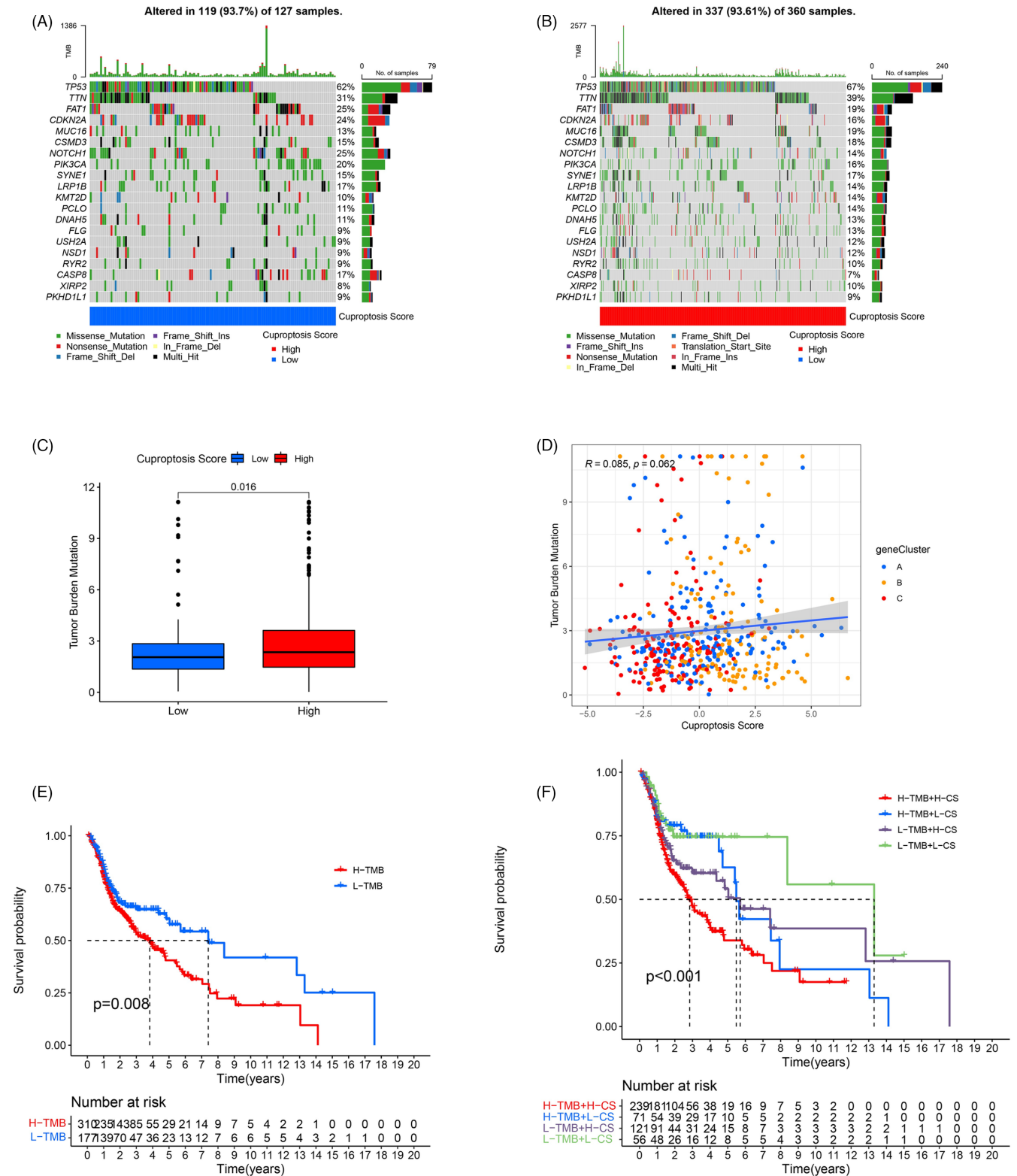
FIGURE 5 Tumor mutation burden analysis. (A) Waterfall plots of mutation in the low-CS group; (B) Waterfall plots of mutation in the high-CS group; (C) Comparison of TMB between two groups; (D) Correlation of TMB, CSs and gene clusters; (E) survival analysis between high and low TMB cohorts; (F) survival analysis for patients based on TMB and CSs.

samples. Concerning the above results, this novel scoring system served as a reliable prognostic biomarker with universal prognostic patterns.

Reportedly, previous studies have determined that TMB plays crucial roles influencing prognosis and immunotherapy response.[25-27] We explored the correlation between CSs and TMB and verified that CS was strongly associated with TMB. Both factors can enhance the risks and shorten the survival time for patients. These results suggested that the CS could be a preferable marker in predicting genomic aberrations.
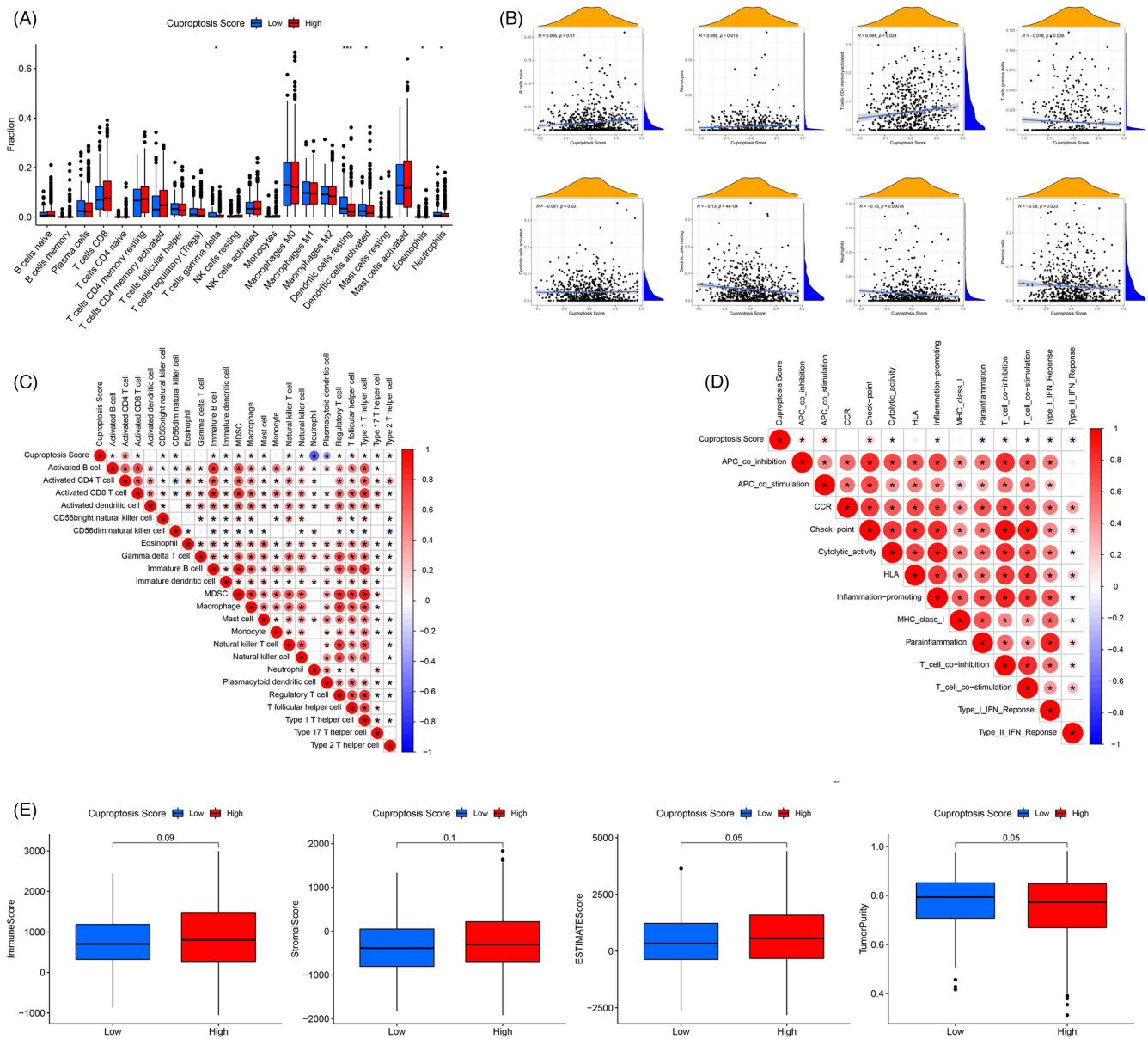
FIGURE 6 TME analysis between the low-CS and high-CS groups. (A) Comparison of immune cell infiltration based on CIBERSORT. (B) Correlation of CSs and immune cells based on CIBERSORT; (C) Correlation of CSs and immune cells according to ssGSEA; (D) Correlation of CSs and immune functions according to ssGSEA; (E) Comparison of TME scores between the two groups.

Importantly, we also assessed the TME of HNSCC patients with the assistance of the CS system. Accordingly, patients with high CSs exhibited more immune cell infiltration, especially CD8+ T cells, which can eliminate tumor cells, disrupt immune tolerance and enhance the immunotherapy response via the PD-1/PD-L1 immune inhibitory axis.[28,29] The correlation analysis of ssGSEA suggested that patients in the high-CS group exhibited a high immunotherapeutic response to ICI therapy, which coincided with the TMB analysis. In addition, the comparative expression of PD-1 and CTLA4 also supported the results that the high-CS group exhibited higher immune checkpoint gene expression.[30,31] Moreover, patients in the low-CS group with an immunosuppressive TME may easily suffer from immune escape based on the TIDE-related scores.[32] Although there were no significant differences in TME scores between the two groups, other immune-related assessments predicted and indicated that patients with high CSs displayed a better immunotherapy response than those with low CSs.[31,33] Given these findings, cuproptosis could affect the response to immunotherapy in HNSCC patients, and CSs can be considered effectively to predict the prognosis of immunotherapy. Moreover, we also explored the relationship between CSs and four therapeutic drugs. The results of drug sensitivity may promote the development of individualized treatment combined with immunotherapy and chemotherapy.[2]

Although we established a novel scoring system to assess the effects of cuproptosis on HNSCC patients, there are several limitations in our study, including the lack of understanding of the mechanism of the effects of cuproptosis patterns on immune infiltration and chemotherapy in HNSCC. Further studies with large samples are required to test the results of these bioinformatics analyses.
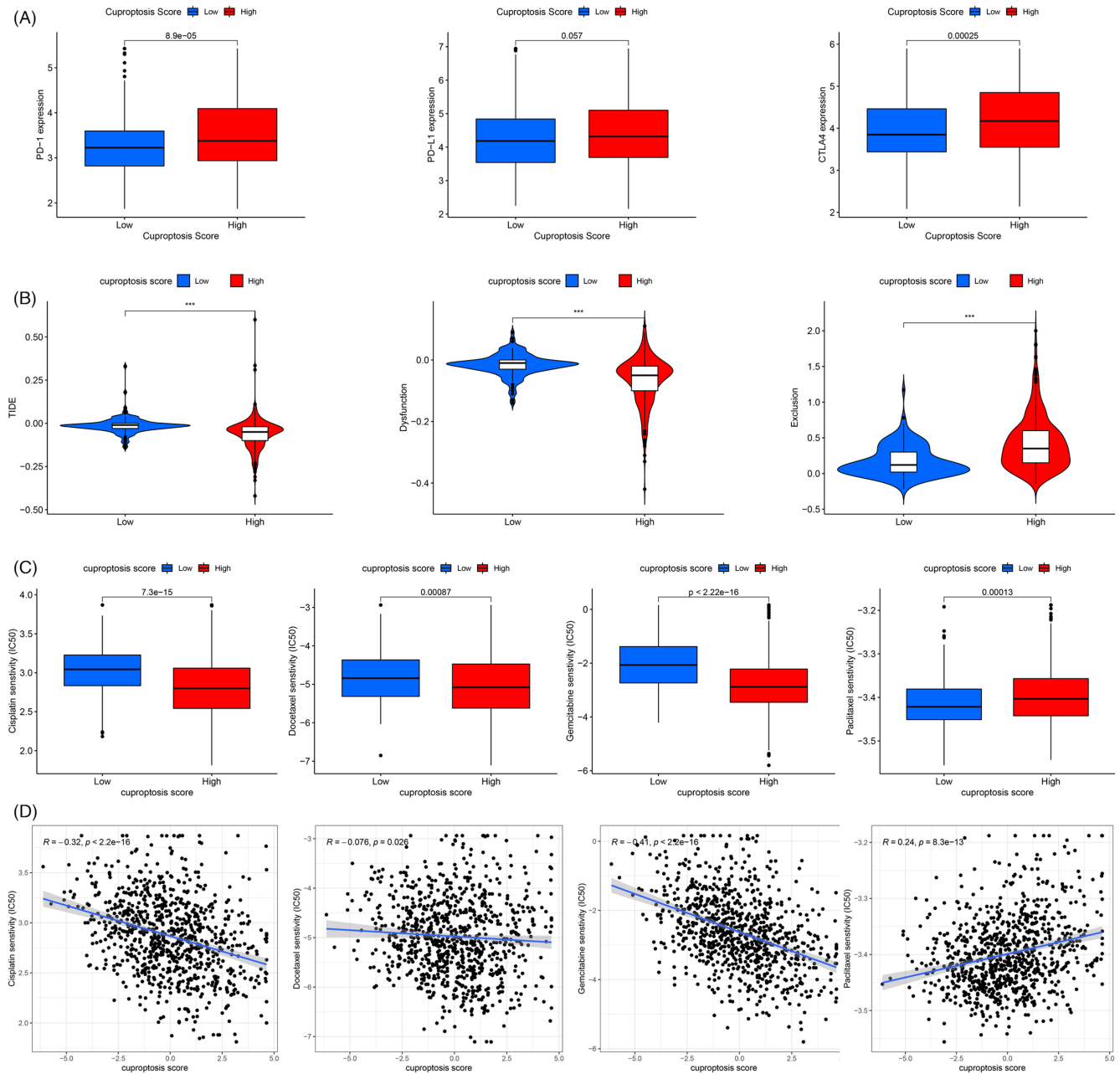
FIGURE 7 Assessment of immunotherapy and chemotherapy. (A) Comparative expression of PD-1, PD-L1 and CTLA4 between the low-CS and high-CS groups; (B) TIDE-related scores in two groups; (C) Comparison of IC50 value of cisplatin, paclitaxel, docetaxel, and gemcitabine; (D) Correlation between CSs and IC50 values of cisplatin, paclitaxel, docetaxel, and gemcitabine.

5 | CONCLUSION

In conclusion, we established a novel cuproptosis-related scoring system to predict the prognosis and immune landscape of HNSCC patients. This signature exhibits satisfactory predictive effects and the potential to guide comprehensive treatment for patients.

AUTHOR CONTRIBUTIONS

All persons designated as the authors have participated sufficiently in the work to take public responsibility for the content of the manuscript.

CONFLICT OF INTEREST

There are no conflicts of interests.

DATA AVAILABILITY STATEMENT

The data used to support the findings of this study comes from the public database and are available from the corresponding author upon request.

ORCID

Juntao Huang https://orcid.org/0000-0002-0206-9365
Chongchang Zhou https://orcid.org/0000-0002-8728-6819

REFERENCES

1. Bray F, Ferlay J, Soerjomataram I, Siegel RL, Torre LA, Jemal A. Global cancer statistics 2018: GLOBOCAN estimates of incidence and mortality worldwide for 36 cancers in 185 countries. *CA Cancer J Clin*. 2018;68:394-424.
2. Huang J, Xu Z, Teh BM, et al. Construction of a necroptosis-related lncRNA signature to predict the prognosis and immune microenvironment of head and neck squamous cell carcinoma. *J Clin Lab Anal*. 2022;36(6):e24480.
3. Kaidar-Person O, Gil Z, Billan S. Precision medicine in head and neck cancer. *Drug Resist Updat*. 2018;40:13-16.
4. Canning M, Guo G, Yu M, et al. Heterogeneity of the head and neck squamous cell carcinoma immune landscape and its impact on immunotherapy. *Front Cell Dev Biol*. 2019;7:52.
5. Samra B, Tam E, Baseri B, Shapira I. Checkpoint inhibitors in head and neck cancer: current knowledge and perspectives. *J Invest Med*. 2018;66:1023-1030.
6. Muzaffar J, Bari S, Kirtane K, Chung CH. Recent advances and future directions in clinical management of head and neck squamous cell carcinoma. *Cancer*. 2021;13:338.
7. Ferris RL, Blumenschein G, Fayette J, et al. Nivolumab for recurrent squamous-cell carcinoma of the head and neck. *N Engl J Med*. 2016;375:1856-1867.
8. Gillison ML, Blumenschein G, Fayette J, et al. CheckMate 141: 1-year update and subgroup analysis of nivolumab as first-line therapy in patients with recurrent/metastatic head and neck cancer. *Oncologist*. 2018;23:1079-1082.
9. Seiwert TY, Burtness B, Mehra R, et al. Safety and clinical activity of pembrolizumab for treatment of recurrent or metastatic squamous cell carcinoma of the head and neck (KEYNOTE-012): an open-label, multicentre, phase 1b trial. *Lancet Oncol*. 2016;17:956-965.
10. Ferris RL, Whiteside TL, Ferrone S. Immune escape associated with functional defects in antigen-processing machinery in head and neck cancer. *Clin Cancer Res*. 2006;12:3890-3895.
11. Deng H, Wei Z, Qiu S, et al. Pyroptosis patterns and immune infiltrates characterization in head and neck squamous cell carcinoma. *J Clin Lab Anal*. 2022;36(4):e24292.
12. Tsvetkov P, Coy S, Petrova B, et al. Copper induces cell death by targeting lipoylated TCA cycle proteins. *Science*. 2022;375:1254-1261.
13. Tang D, Chen X, Kroemer G. Cuproptosis: a copper-triggered modality of mitochondrial cell death. *Cell Res*. 2022;32:417-418.
14. Cobine PA, Moore SA, Leary SC. Getting out what you put in: copper in mitochondria and its impacts on human disease. *Biochim Biophys Acta Mol Cell Res*. 2021;1868:118867.
15. Hänzelmann S, Castelo R, Guinney J. GSVA: gene set variation analysis for microarray and RNA-seq data. *BMC Bioinformatics*. 2013;14:7.
16. Zhang B, Wu Q, Li B, Wang D, Wang L, Zhou YL. m6A regulator-mediated methylation modification patterns and tumor microenvironment infiltration characterization in gastric cancer. *Mol Cancer*. 2020;19(1):53.
17. Yang Z, Ming X, Huang S, Yang M, Zhou X, Fang J. Comprehensive analysis of mA regulators characterized by the immune cell infiltration in head and neck squamous cell carcinoma to aid immunotherapy and chemotherapy. *Front Oncol*. 2021;11:764798.
18. Snyder AG, Hubbard NW, Messmer MN, et al. Intratumoral activation of the necroptotic pathway components RIPK1 and RIPK3 potentiates antitumor immunity. *Sci Immunol*. 2019;4:eaaw2004.
19. Yang Z, Jiang B, Wang Y, et al. 2-HG inhibits necroptosis by stimulating DNMT1-dependent hypermethylation of the RIP3 promoter. *Cell Rep*. 2017;19:1846-1857.
20. Yatim N, Jusforgues-Saklani H, Orozco S, et al. RIPK1 and NF-κB signaling in dying cells determines cross-priming of CD8+ T cells. *Science*. 2015;350:328-334.
21. Frankel T, Lanfranca MP, Zou W. The role of tumor microenvironment in cancer immunotherapy. *Adv Exp Med Biol*. 2017;1036:51-64.
22. Pitt JM, Marabelle A, Eggermont A, Soria JC, Kroemer G, Zitvogel L. Targeting the tumor microenvironment: removing obstruction to anticancer immune responses and immunotherapy. *Ann Oncol*. 2016;27:1482-1492.
23. Leemans CR, Snijders PJF, Brakenhoff RH. The molecular landscape of head and neck cancer. *Nat Rev Cancer*. 2018;18:269-282.
24. Network CGA. Comprehensive genomic characterization of head and neck squamous cell carcinomas. *Nature*. 2015;517:576-582.
25. Liu L, Bai X, Wang J, et al. Combination of TMB and CNA stratifies prognostic and predictive responses to immunotherapy across metastatic cancer. *Clin Cancer Res*. 2019;25:7413-7423.
26. Zhang L, Li B, Peng Y, et al. The prognostic value of TMB and the relationship between TMB and immune infiltration in head and neck squamous cell carcinoma: a gene expression-based study. *Oral Oncol*. 2020;110:104943.
27. George S, Miao D, Demetri GD, et al. Loss of PTEN is associated with resistance to anti-PD-1 checkpoint blockade therapy in metastatic uterine leiomyosarcoma. *Immunity*. 2017;46:197-204.
28. Duan Q, Zhang H, Zheng J, Zhang L. Turning cold into hot: firing up the tumor microenvironment. *Trends Cancer*. 2020;6:605-618.
29. McGranahan N, Furness AJS, Rosenthal R, et al. Clonal neoantigens elicit T cell immunoreactivity and sensitivity to immune checkpoint blockade. *Science*. 2016;351:1463-1469.
30. Yan L, Song X, Yang G, Zou L, Zhu Y, Wang X. Identification and validation of immune infiltration phenotypes in laryngeal squamous cell carcinoma by integrative multi-omics analysis. *Front Immunol*. 2022;13:843467.
31. Zheng Y, Tian H, Zhou Z, et al. A novel immune-related prognostic model for response to immunotherapy and survival in patients with lung adenocarcinoma. *Front Cell Dev Biol*. 2021;9:651406.
32. Jiang P, Gu S, Pan D, et al. Signatures of T cell dysfunction and exclusion predict cancer immunotherapy response. *Nat Med*. 2018;24:1550-1558.
33. Immunotherapy in head and neck cancers: a new challenge for immunologists, pathologists and clinicians. *Cancer Treat Rev*. 2018;65:54-64.

SUPPORTING INFORMATION

Additional supporting information can be found online in the Supporting Information section at the end of this article.